Journal of Power Sources 202 (2012) 384–388

Contents lists available at SciVerse ScienceDirect

Journal of Power Sources

journal homepage: www.elsevier.com/locate/jpowsour

Short communication

Synergism of ionic liquid and surfactant molecules in the growth of $LiFePO_4$ nanorods and the electrochemical performances

Fei Teng[a,*], Mindong Chen[a,*], Guiqing Li[a], Yang Teng[c], Tongguang Xu[d], Sun-il Mho[b], Xia Hua[a]

[a] Jiangsu Key Laboratory of Atmospheric Environment Monitoring and Pollution Control, Innovative Research Laboratory of Clean Energy, Environmental Catalysis & New Materials, School of Environmental Science and Engineering, Nanjing University of Information Science & Technology, 219 Ningliu Road, Nanjing 210044, China
[b] Division of Energy System Research, Ajou University, Suwon 443-749, Republic of Korea
[c] Department of Information Science, Suzhou Institute of Trade and Commerce, Suzhou 215009, PR China
[d] Beijing Cigarette Factory, Beijing 101121, China

ARTICLE INFO

Article history:
Received 23 August 2011
Received in revised form
19 November 2011
Accepted 21 November 2011
Available online 1 December 2011

Keywords:
Lithium iron phosphate
Nanorods
Ionic liquid
Charge and discharge
Capability

ABSTRACT

In this work, the $LiFePO_4$ nanorods are synthesized in an ionic liquid (IL) in the presence of a surfactant. The samples are characterized by X-ray diffraction, scanning electron microscopy, high resolution transmission electron microscopy, electron diffraction and nitrogen adsorption. The as-obtained $LiFePO_4$ nanorods in the IL have the diameter of about 200 nm and the length of 1–2 μm; but the aggregated $LiFePO_4$ microparticles are obtained in the aqueous solution. The results show that a higher temperature and a longer duration are needed in the IL than in the aqueous solution for the formation of $LiFePO_4$; that both IL and the surfactant play the key roles in the formation of $LiFePO_4$ nanorods. Furthermore, their charge and discharge properties are investigated. The $LiFePO_4$ nanorods show a higher discharge capacity (150 at 1*C* rate) and a higher rate capability than the aggregated particles (133 mAh g^{-1}). The adopted IL approach may provide a "green" route to achieve excellent battery materials.

1. Introduction

$LiFePO_4$ is one of the most promising cathode materials in electric and plug-in hybrid vehicles, which demand both fast charging and safety regulation [1,2]. Due to the stable three-dimensional framework of phospho-olivine, $LiFePO_4$ is much safer than the other cathode materials upon overcharging or overdischarging [3]. However, the bulk $LiFePO_4$ generally shows the limited rate capability because of the low electronic conductivity and lithium ion diffusion rate [2,4]. It has been demonstrated that the performances of $LiFePO_4$ cathode can be improved by the particle size and morphology [5–11]. For example, Huang et al. [5] reported that the $LiFePO_4$ nanorods had a high discharge capacity and a stable cyclabilty after 20 cycles, and they ascribed the improved performances to the nanorod shape. Gangulibabu et al. [6] studied the lithium intercalation behavior of $LiFePO_4$/C. They concluded that the excellent rate capability resulted from the synergistic effect of the nanorod morphology and super P carbon coating. Compared with bulk or microsized electrode materials, the nanosized materials can provide the shorter transport path for lithium ions and electrons, and larger electrode/electrolyte interface, which lead to higher charge and discharge rates [5,6]. The results suggest that the morphologies of electrode materials have a significant influence on the electrochemical performances. Moreover, the nanorod/nanowire electrodes are reported to have better strain endurance capability than the particle-based ones in the lithium ion insertion and extraction processes [12–15]. For example, Chan et al. [15] have demonstrated that silicon nanowires had a higher stability than silicon powders in the charge and discharge processes. Hence, it is desirable to acquire the nanorod electrode materials.

Ionic liquids (ILs), which have high thermal stability and negligible vapor pressure, have attracted increasing interests due to the applications in batteries, supercapacitors, to name only a few [16–18]. Ionothermal synthesis provides a promising strategy to control material structures, in which ILs can act as both solvents and templates [19]. However, ionic liquids have been widely used in organic synthesis, fewer reports can be available in the field of inorganic synthesis [20,21]. Recently, the $LiFePO_4$ nanoplates [20] and nanoparticles [21] are prepared by the ionothermal method, which show the excellent electrochemical performances. Nevertheless, the ionothermal synthesis of $LiFePO_4$ nanorods has not been available so far.

In this work, we explored the synthesis of $LiFePO_4$ nanorods in IL. The samples were characterized by XRD, SEM, HRTEM and N_2 adsorption. The effects of IL and surfactant on the sample were mainly investigated. The charge and discharge properties of the

* Corresponding authors. Tel.: +86 25 5976 9899; fax: +86 25 5976 9899.
E-mail addresses: tfwd@163.com (F. Teng), Chenmd_nj@nuist.edu.cn (M. Chen).

0378-7753/$ – see front matter © 2011 Elsevier B.V. All rights reserved.
doi:10.1016/j.jpowsour.2011.11.063

samples were also measured. Because of the high thermal stability and negligible volatility, the reported ionothermal approach could be accepted as an "green" route, compared with solvothermal methods.

2. Experimental

2.1. Chemicals

In this work, all chemicals were used as purchased without further purification. $FeSO_4{\cdot}7H_2O$, LiOH, H_3PO_4 (85 wt%), L(+)-Ascorbic acid, 1-butyl-3-methylimidazolium tetrafluoroborate (99.5%, [BuMIm][BF_4], $\rho = 1.38\ g\ mL^{-1}$) and dodecyl benzene sulphonic acid sodium (SDBS, 99.5%) were purchased from Sigma–Aldrich.

2.2. Preparation of the samples

The $LiFePO_4$ nanorods were synthesized in [BuMIm][BF_4], in which L-Ascorbic acid was added as a reducing agent to prevent the oxidation of Fe(II). Typically, 0.001 mol of $FeSO_4{\cdot}7H_2O$ was used in the experiment. The measured amounts of $FeSO_4{\cdot}7H_2O$, LiOH, H_3PO_4, L-Ascorbic acid and SDBS with the molar ratios of 3:1:1:1:1 were added into 12 mL of [BuMIm][BF_4]. After intensive magnetic stirring overnight, the suspension was transferred into a 20-mL Teflon®-lined stainless steel autoclave, then heated to 240 °C and kept at 240 °C for 20 h. After being cooled naturally to room temperature, the solids were separated, washed and dried at 80 °C for 24 h in a vacuum. In order to investigate the formation of $LiFePO_4$, the samples were also prepared at different temperatures and durations while all the other conditions were the same as above. Herein, the samples obtained at 160 °C/20 h, 200 °C/20 h, 240 °C/5 h, 240 °C/10 h, 240 °C/20 h and 240 °C/30 h were designated as S1, S2, S3, S4, S5 and S6, respectively.

In addition, the $LiFePO_4$ sample was also prepared in aqueous medium at 160 °C/6 h while all the other conditions were same as above. The as-prepared sample was designated as S7. The as-synthesized samples at different conditions were summarized in Table 1.

2.3. Characterization

The morphologies of the samples were observed on a scanning electron microscope (SEM, Hitachi SU-1510) with an acceleration voltage of 15 keV. The samples were coated with 5-nm-thick gold layer before observations,. The structure properties of the samples were determined by using high-resolution transmission electron microscopy (HRTEM, JEOL JEM-2100F) equipped with an electron diffraction (ED) attachment with an acceleration voltage of 200 kV. The phase compositions of the samples were determined by powder X-ray diffractometer (Rigaku D/max-2550VB), using graphite monochromatized Cu Kα radiation ($\lambda = 0.154$ nm), operating at 40 kV and 50 mA. The XRD patterns were obtained in the range of 10–60° (2θ) at a scanning rate of $5°\ min^{-1}$. A nitrogen adsorption isotherm was performed at 77 K and $<10^{-4}$ bar on a Micromeritics ASAP2010 gas adsorption analyzer. Each sample was degassed at 150 °C for 5 h before the measurement. Surface area was calculated by the BET (Brunauer–Emmett–Teller) method.

2.4. Charge and discharge properties

The charge and discharge performances of the samples were conducted with a CR2032 coin cell assembled in an argon-filled glove box. The working electrode consisted of 75 wt% $LiFePO_4$ powder, 15 wt% acetylene black and 10 wt% polyvinylidene fluoride (PVDF) binder. N-methyl-2-pyrrolidinon (NMP) was used as solvent to obtain a slurry, which was cast onto the aluminum current collector and achieved loading of $\sim 1\ mg\ cm^{-2}$. The working electrode was then dried overnight under vacuum at 120 °C. A Teflon Celgard separator (#2400) was used to separate the working electrode and a lithium foil counter electrode. The used electrolyte was 1 M $LiPF_6$ solution in ethylene carbonate (EC)/dimethyl carbonate (DMC)/diethyl carbonate (DEC) (1:1:1, in wt%). The charge and discharge measurements of the assembled coin cell was performed on an Arbin BT2000 system in the voltage range of 2.0–4.2 V at different C rates of 1, 2 and 4C ($C = 170\ mA\ g^{-1}$) at 25 °C.

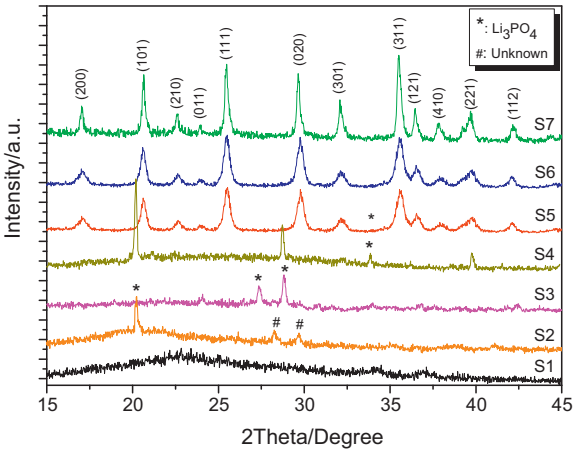

Fig. 1. XRD patterns of the prepared samples corresponding to those in Table 1.

3. Results and discussion

3.1. The growth of $LiFePO_4$ nanorods in IL

Table 1 presents the as-synthesized samples at different conditions and Fig. 1 shows their XRD patterns. S1 shows an amorphous phase. S2 is mainly composed of Li_3PO_4 and the unknown crystalline phases. It is clear that $LiFePO_4$ crystals cannot form at the low temperatures (160 and 200 °C). At 240 °C, the diffraction peaks of S5 can be well indexed to the phase-pure $LiFePO_4$, referring to JCPDS No. 81-1173. The results indicate that a high temperature is essential for the formation of $LiFePO_4$. The effect of reaction duration on the formation of $LiFePO_4$ is also investigated. At 240 °C for 5 and 10 h, no diffraction peaks of $LiFePO_4$ can be observed, but the diffraction peaks of Li_3PO_4 appear obviously for both S3 and S4. When the reaction duration is extended to 20 and 30 h, both S5 and S6 are single-phase $LiFePO_4$. Compared with S5, the peak intensities of S6 do not significantly increase. Calculated by Scherrer's equation ($D = 0.89\lambda/\beta\cos\theta$) from the full-width-at-half-maximum (β) of the (0 2 0) peak, the mean crystal sizes of both S5 and S6 are 188.6 and 189.1 nm, respectively, indicating that the $LiFePO_4$ crystals do not significantly grow any more. For comparison, the phase-pure $LiFePO_4$ crystals (S7) are obtained in an aqueous solution under hydrothermal conditions. Basing on the (0 2 0) peak, the mean crystal size of S7 is calculated to be 255.3 nm by Scherrer's equation. It is clear that the formation temperature of $LiFePO_4$ crystals in the aqueous solution is lower than that in the IL. This indicates that the reaction medium has a significant influence on the crystallization and growth of $LiFePO_4$.

The morphologies of S5, S6 and S7 are characterized by SEM. It can be observed from Fig. 2a and b that the $LiFePO_4$ nanorods are obtained in the IL (S5, S6), which have the diameters of ca. 200 nm and the lengths of ca. 1–2 μm. In the aqueous solution, however, the aggregated microparticles are obtained (S7), which have the sizes of 1–2 μm. The contrast experiment (Fig. 1S of supporting

Table 1
The preparation conditions, phase compositions, particle shapes and surface areas of the samples.

Sample[a]	T/t (°C/h)	SDBS/Fe[b]	Phases compositions	Particle shape[c]	Surface area ($m^2\ g^{-1}$)[d]
S1	160/20	1/1	Amorphous	/	/
S2	200/20	1/1	Li_3PO_4, unknown phase	/	/
S3	240/5	1/1	Li_3PO_4	/	/
S4	240/10	1/1	Li_3PO_4	/	/
S5	240/20	1/1	$LiFePO_4$	Nanorods	22.5
S6	240/30	1/1	$LiFePO_4$	Nanorods	21.2
S7	160/6	1/1	$LiFePO_4$	Aggregated particles	5.8

[a] *Notes*: S1–S6, prepared in ionic liquid; S7, prepared by a hydrothermal method.
[b] Molar ratio.
[c] From SEM observation.
[d] Calculated by the BET method.

information) shows that in the absence of SDBS, the as-obtained $LiFePO_4$ particles are not nanorods, but the irregular particles. It is clear that SDBS plays a key role in the growth of $LiFePO_4$ nanorods.

Typically, S5 is further characterized by HRTEM. Fig. 2d also shows that the $LiFePO_4$ nanorods have the diameter of about 200 nm, which is consistent to the SEM result. In the inset of Fig. 2e presents the selected area electron diffraction (ED) patterns taken on the tip of the nanorod. The clear diffraction spots are determined to be (1 6 2), (0 2 2), (1 2 2) and (1 3 1) planes of $LiFePO_4$, respectively. The ED patterns reveal the single-crystalline nature of the $LiFePO_4$ nanorods. Fig. 2e shows the fringe lattice image of the sample. The *d*-spacing is determined to be 0.285 nme, corresponding to the (0 2 0) plane of $LiFePO_4$, suggesting that the nanorods preferentially grow along the [0 2 0] direction.

The above results show that a higher energy is required for the formation of $LiFePO_4$ in IL than that in water. It seems that the reaction medium has a significant influence on the formation of $LiFePO_4$. The specific properties of IL are mainly taken into account. It has been reported that a water/IL system is not a homogeneous system, in which most of ILs are self-associated as tight ion pair in IL-rich region, and most of water molecules are self-associated in water-rich region [22]. In addition to both extreme cases, ionic liquid strongly interact with water molecules through hydrogen bonding [22,23]. Due to the large van der Waal force and hydrogen bonding, ILs have the high viscosity. As a result, the diffusion rates of ions in ILs are lower than those in water. Based on Recham's work [20], $LiFePO_4$ is believed to form through the following chemical reaction:

$$Fe^{2+} + Li_3PO_4 \rightarrow LiFePO_4 + 2Li^+ \quad (1)$$

in which Fe(II) may react with Li_3PO_4 and trigger the precipitation of $LiFePO_4$. Therefore, a high temperature is essential for the formation of $LiFePO_4$ in the IL. On the other hand, about 1.2 wt% of water is contained in the IL/water mixture by the Karl–Fischer method, which results from the precursor chemicals. We believe that the small amount of water facilitates the formation of $LiFePO_4$. It has been demonstrated that a small amount of water is essential for the formation of $ZnIn_2S_4$ [24]. Liu et al. [25] report that the high-crystallinity anatase TiO_2 can be obtained at high water contents. Wragg et al. further report that the coexistence of water and IL plays a critical role in the formation of anatase, but at higher water contents, the templating effect of ILs is poor [26]. A suitable amount of water facilitates the formation of crystals through a dissolution-crystallization mechanism [27].

A plausible formation mechanism is proposed, as shown in Fig. 3. It is well known that the particle size and morphology can be controlled effectively in the presence of surfactant [28–31]. The growths of some crystal planes may be significantly prevented by the strongly binding with or adsorbing SDBS molecules, but the growth rates of the other crystal planes may be fast due to the weakly binding with or adsorbing SDBS molecules. As a result, the $LiFePO_4$ nanorods can form. Moreover, the unlimited growth of the

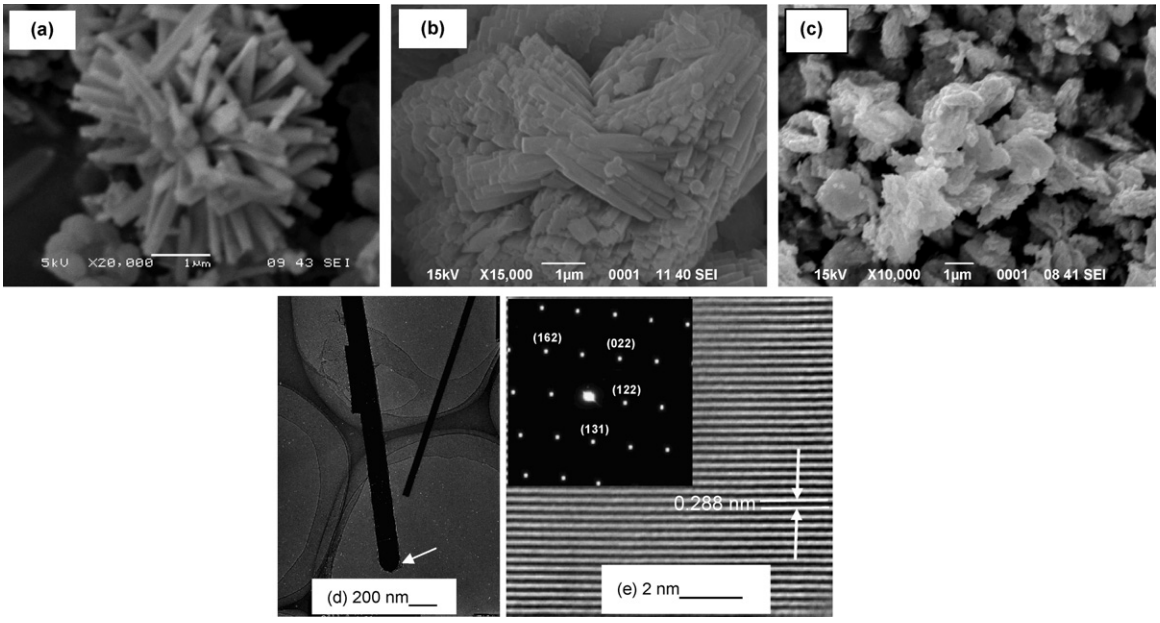

Fig. 2. SEM and HRTEM images of the samples: (a–c) SEM images of S5, S6 and S7; (d) TEM image of S5; (e) lattice fringe (the inset of ED patterns) of S5.

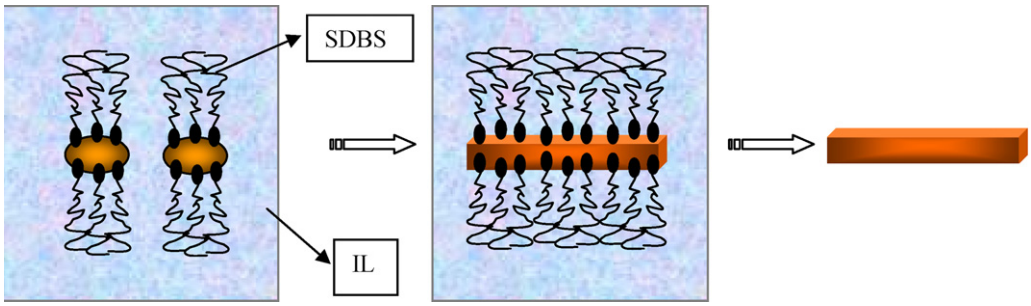

Fig. 3. The proposed formation mechanism of the $LiFePO_4$ nanorods: IL, Ionic liquid; SDBS, surfactant molecules.

$LiFePO_4$ nanorods may also be restrained by the self-associated network of ILs. It has been reported that the ionic liquids can act both as solvents and stabilizers in the ionothermal process [32]. Therefore, the $LiFePO_4$ nanorods can be templated simultaneously by SDBS and IL molecules.

3.2. Charge and discharge performances of the $LiFePO_4$ nanorods

Fig. 4a shows the initial charge and discharge curves of S5, S6 and S7 in the cutoff voltage range of 2.0–4.2 at 1*C* rate. A typical flat plateaus at 3.4–3.5 V can be observed in the charge and discharge processes, representing the insertion and extraction behaviors of Li ions. This flat plateau can be attributed to the two-phase reaction as follows [33]:

$$LiFePO_4 \leftrightarrow (1-y)LiFePO_4 + yFePO_4 + yLi^+ + ye \quad (2)$$

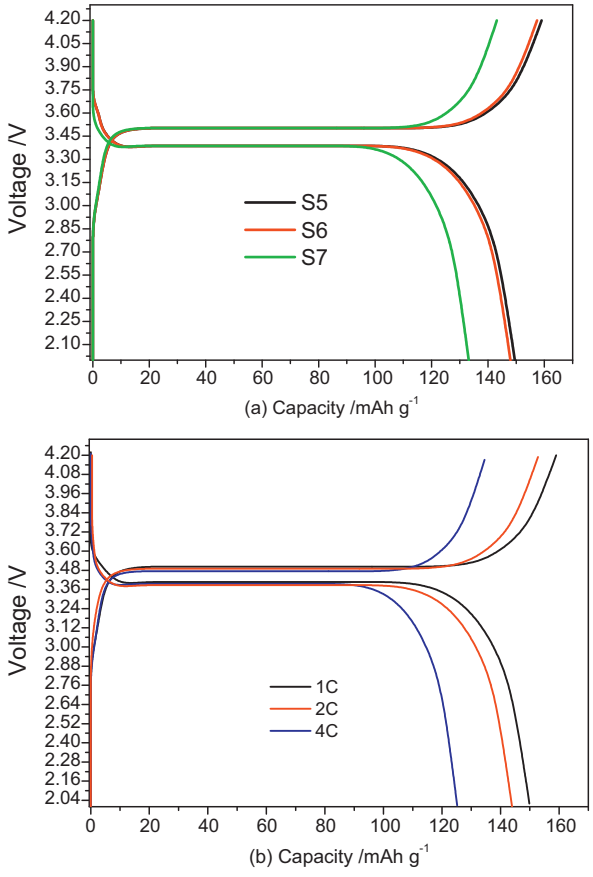

Fig. 4. (a) The initial charge and discharge curves of the $LiFePO_4$ samples at 1*C* rate and (b) The charge and discharge profiles of S5 at different C rates between 2.0 and 4.2 V.

The discharge capacities of S5 and S6 are 150 and 148 mAh g^{-1}, and their coulombic efficiencies are 94.33% vs. 94.26%, respectively. The discharge capacity and coulombic efficiency of S7 are 133 mAh g^{-1} and 93%, which are lower than those of S5 and S6, respectively. The high discharge capacities of the $LiFePO_4$ nanorods (S5,S6) are closely related to the textural properties (Table 1). The BET areas of S5 and S6 are 22.5 and 21.2 m^2 g^{-1}, respectively, which are larger than that (5.8 m^2 g^{-1}) of S7. The large surface areas of the $LiFePO_4$ nanorods favor the fast intercalation of lithium ions.

Fig. 4b shows the rate capability of S5. At 1*C*, 2*C* and 4*C* rates, the discharge capacities of S5 are 150, 144 and 125 mAh g^{-1}, respectively. Compared with the theoretical capacity (170 mAh g^{-1}) of $LiFePO_4$, 88%, 85% and 73% of theoretical capacity are reached at 1*C*, 2*C*, 4*C* rates for S5, respectively. Moreover, about 96% and 83% of the discharge capacity at 1*C* rate are retained at 2*C* and 4*C* rates, respectively, indicating the excellent rate capability. The rate capabilities of S6 and S7 are given in Fig. 2S (Supporting information). S6 also shows the good rate capability. For S7, only 78%,72% and 61% of theoretical capacity are reached at 1*C*, 2*C*, 4*C* rates. At 4*C* rate, only 69.9% of 1*C* capacity is retained. The high rate capabilities of S5 and S6 are closely relative to the $LiFePO_4$ nanorods, which have the short diffusion path of lithium ions. Martin et al. have reported that the nanofiber morphology mitigates the slow transport problem of lithium ions, because the diffusion distance of lithium ions within the electrode material can be minimized [34,35].

Fig. 5 presents the cyclability of S5 at 1*C*, 2*C* and 4*C* rates. After 50 cycles, the discharge capacity of S5 has not faded obviously. The good cyclability may be closely relative to the nanorod morphology. It is generally accepted that one-dimensional electrode materials can endure large volume variations caused by the insertion/extraction of lithium ions. Chan et al. [15] have reported that the silicon nanowires had a higher stability than the silicon powders in the charge and discharge processes. Huang et al.

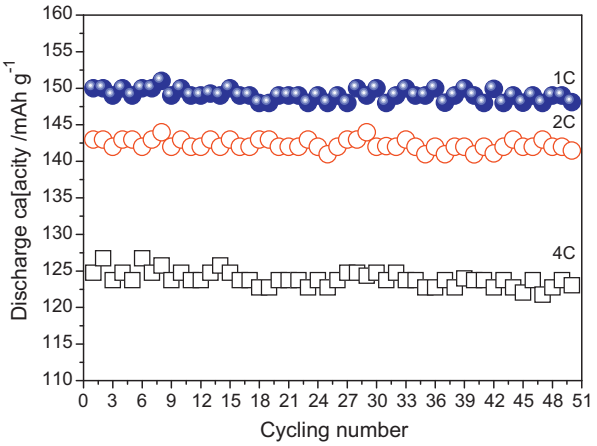

Fig. 5. Cyclability of S5 at different C rates between 2.0 and 4.2 V.

have reported [5] that the $LiFePO_4$ nanorod maintained a stable discharge capacity of 132 mAh g^{-1} at 0.5 C rate after 20 cycles. Gangulibabu et al. [6] also reported that $LiFePO_4$/super P composite cathode delivered a discharge capacity of 160 mAh g^{-1} at C/20 with an excellent capacity retention (95%) up to 50 cycles, and delivered a capacity of 122 mAh g^{-1} at 1 C rate. The reported $LiFePO_4$ nanorods in our study show a higher discharge capability than the aforementioned results. Summarily, the $LiFePO_4$ nanorods can be expected to be a useful cathode material for lithium-ion battery.

4. Conclusions

The growth of the $LiFePO_4$ nanorods can be controlled simultaneously by both self-associated ILs and surfactant. A high temperature and a long duration are essential for the formation of $LiFePO_4$ in IL. The $LiFePO_4$ nanorods have a higher rate capability and a higher cyclability than the large irregular particles obtained in aqueous solution. The adopted approach may provide a "green" route to achieve the excellent battery materials.

Acknowledgments

This work is financially supported by National Science Foundation of China (20943004), Six Talent Climax Foundation of Jiangsu (20100292), "333" Outstanding Youth Scientist Foundation (20110211) of Jiangsu and the Korea Research Foundation Grant (KRF-2007-412-J04003).

Appendix A. Supplementary data

Supplementary data associated with this article can be found, in the online version, at doi:10.1016/j.jpowsour.2011.11.063.

References

[1] A.K. Padhi, K.S. Nanjundaswamy, J.B. Goodenough, J. Electrochem. Soc. 144 (1997) 1188.
[2] J.-M. Tarascon, M. Armand, Nature 414 (2001) 359.
[3] P.S. Herle, B. Ellis, N. Coombs, L.F. Nazar, Nat. Mater. 3 (2004) 147.
[4] S.Y. Chung, J.T. Bloking, Y.M. Chiang, Nat. Mater. 1 (2002) 123.
[5] X. Huang, S. Yan, H. Zhao, L. Zhang, R. Guo, C. Chang, X. Kong, H. Han, Mater. Charact. 61 (2010) 720.
[6] Gangulibabu, N. Kalaiselvi, D. Bhuvaneswari1, C.H. Doh, Int. J. Electrochem. Sci. 5 (2010) 1597.
[7] A. Yamada, S.C. Chung, K. Hinokuma, J. Electrochem. Soc. 148 (3) (2001) A224.
[8] C. Delacourt, P. Poizot, M. Morcrette, J.M. Tarascon, C. Masquelier, Chem. Mater. 16 (2004) 93.
[9] C.R. Sides, F. Croce, V.Y. Young, C.R. Martin, B. Scrosati, Electrochem. Solid State Lett. 8 (2005) A484.
[10] B. Kang, G. Ceder, Nature 458 (2009) 190.
[11] F. Teng, S. Santhanagopalan, A. Asthana, X. Geng, S. Mho, R. Shahbazian-Yassar, D. Meng, J. Cryst. Growth 312 (2010) 3493.
[12] A.S. Aricò, P. Bruce, B. Scrosati, J.M. Tarascon, W. Van Schalkwijk, Nat. Mater. 4 (5) (2005) 366.
[13] D. Wang, H. Buqa, M. Crouzet, G. Deghenghi, T. Drezen, I. Exnar, N.H. Kwon, J.H. Miners, L. Poletto, M. Grätzel, J. Power Sources 189 (2009) 624.
[14] G. Wang, X. Shen, J. Yao, J. Power Sources 189 (2009) 543.
[15] C.K. Chan, R.N. Patel, M.J. O'Connel, B.A. Korgel, Y. Cui, ACS Nano 4 (3) (2010) 1443.
[16] M. Armand, F. Endres, D.R. MacFarlane, H. Ohno, B. Scrosati, Nat. Mater. 8 (2009) 621.
[17] E.R. Parnham, R.E. Morris, Acc. Chem. Res. 40 (2007) 1005.
[18] E. Azaceta, R. Tena-Zaera, R. Marcilla, S. Fantini, J. Echeberria, J.A. Pomposo, H. Grande, D. Mecerreyes, Electrochem. Commun. 11 (2009) 2184.
[19] V. Lair, J. Sirieix-Plenet, L. Gaillon, C. Rizzi, A. Ringuede, Electrochim. Acta 56 (2010) 784.
[20] N. Recham, L. Dupont, M. Courty, K. Djellab, D. Larcher, M. Armand, J.-M. Tarascon, Chem. Mater. 21 (2009) 1096.
[21] Y. Chen, J.-M. Tarascon, C. Guéry, Electrochem. Commun. 13 (2011) 673.
[22] X. Zhu, Y. Wang, H. Li, AIChE J. 55 (2009) 198.
[23] W. Liu, T. Zhao, Y. Zhang, H. Wang, M. Yu, J. Solution Chem. 35 (2006) 1337.
[24] C. Li, H. Li, L. Han, C. Li, S. Zhang, Mater. Lett. 65 (2011) 2537.
[25] Y. Liu, P.-I. Liu, L.-C. Chung, H. Shao, M.-S. Huang, R.-Y. Horng, S.W. Yu, A.C.-M. Yang, M.-C. Chang, J. Mater. Sci. 46 (2011) 4826.
[26] D.S. Wragg, A.M.Z. Slawin, R.E. Morris, Solid State Sci. 11 (2009) 411.
[27] Y. Liu, M. Chang, H. Shao, M. Huang, A.C.-M. Yang, J. Mater. Sci. 45 (2010) 369.
[28] J. Xiang, H. Cao, J.H. Warner, A.A.R. Watt, Cryst. Growth Des. 8 (2008) 4583.
[29] G. Zhou, M. Lu, Z. Yang, F. Tian, Y. Zhou, A. Zhang, Cryst. Growth Des. 7 (2007) 187.
[30] Y. Huang, W. Wang, H. Liang, H. Xu, Cryst. Growth Des. 9 (2009) 858.
[31] G. Leem, S. Sarangi, S. Zhang, I. Rusakova, A. Brazdeikis, D. Litvinov, T.R. Lee, Cryst. Growth Des. 8 (2009) 32.
[32] K. Biswas, C.N.R. Rao, Chem. Eng. J. 13 (2007) 6123.
[33] P. Gibot, M.C. Cabanas, L. Laffont, S. Levasseur, P. Carlach, S. Hamelet, J.M. Tarascon, C. Masquelier, Nat. Mater. 7 (2008) 741.
[34] C.J. Patrissi, C.R. Martin, J. Electrochem. Soc. 146 (1999) 3176.
[35] N. Meetong, H. Huang, W.C. Carter, Y.M. Chiang, Electrochem. Solid State Lett. 10 (2007) A134.